Contributions From Cloud Morphological Changes to the Interannual Shortwave Cloud Feedback Based on MODIS and ISCCP Satellite Observations

Ivy Tan, Mark D. Zelinka, Quentin Coopman, Brian H. Kahn, Lazaros Oreopoulos, George Tselioudis, Daniel T. Mccoy, Ninghui Li

JGR Atmospheres

RESEARCH ARTICLE
10.1029/2023JD040540

Contributions From Cloud Morphological Changes to the Interannual Shortwave Cloud Feedback Based on MODIS and ISCCP Satellite Observations

Ivy Tan[1], Mark D. Zelinka[2], Quentin Coopman[1,3], Brian H. Kahn[4], Lazaros Oreopoulos[5], George Tselioudis[6], Daniel T. McCoy[7], and Ninghui Li[1]

[1]McGill University, Montreal, QC, Canada, [2]Lawrence Livermore National Laboratory, Livermore, CA, USA, [3]University Lille, CNRS, UMR 8518 - LOA - Laboratoire d'Optique Atmospherique, Lille, France, [4]Jet Propulsion Laboratory, California Institute of Technology, Pasadena, CA, USA, [5]NASA GSFC, Earth Sciences Division, Greenbelt, MD, USA, [6]NASA GISS, New York, NY, USA, [7]University of Wyoming, Laramie, WY, USA

Key Points:

- MODIS satellite observations indicate that in the Southern Ocean the interannual cloud optical depth feedback is slightly positive
- More frequently occurring thin low-level clouds and fewer storm-track clouds contribute to a positive feedback in the Southern Ocean
- Strengthened near-surface winds contribute to a negative low-level cloud feedback in the Southern Ocean

Supporting Information:

Supporting Information may be found in the online version of this article.

Correspondence to:

I. Tan,
ivy.tan@mcgill.ca

Citation:

Tan, I., Zelinka, M. D., Coopman, Q., Kahn, B. H., Oreopoulos, L., Tselioudis, G., et al. (2024). Contributions from cloud morphological changes to the interannual shortwave cloud feedback based on MODIS and ISCCP satellite observations. *Journal of Geophysical Research: Atmospheres*, *129*, e2023JD040540. https://doi.org/10.1029/2023JD040540

Received 3 DEC 2023
Accepted 28 MAR 2024

Abstract The surface temperature-mediated change in cloud properties, referred to as the cloud feedback, continues to dominate the uncertainty in climate projections. A larger number of contemporary global climate models (GCMs) project a higher degree of warming than the previous generation of GCMs. This greater projected warming has been attributed to a less negative cloud feedback in the Southern Ocean. Here, we apply a novel "double decomposition method" that employs the "cloud radiative kernel" and "cloud regime" concepts, to two data sets of satellite observations to decompose the interannual cloud feedback into contributions arising from changes within and shifts between cloud morphologies. Our results show that contributions from the latter to the cloud feedback are large for certain regimes. We then focus on interpreting how both changes within and between cloud morphologies impact the shortwave cloud optical depth feedback over the Southern Ocean in light of additional observations. Results from the former cloud morphological changes reveal the importance of the wind response to warming increases low- and mid-level cloud optical thickness in the same region. Results from the latter cloud morphological changes reveal that a general shift from thick storm-track clouds to thinner oceanic low-level clouds contributes to a positive feedback over the Southern Ocean that is offset by shifts from thinner broken clouds to thicker mid- and low-level clouds. Our novel analysis can be applied to evaluate GCMs and potentially diagnose shortcomings pertaining to their physical parameterizations of particular cloud morphologies.

Plain Language Summary Climate models project that rising levels of greenhouse gas emissions will raise Earth's global mean surface air temperature. However, the amount of warming to be expected remains highly uncertain. A main underlying cause for this uncertainty is the representation of atmospheric clouds in these models. In particular, the response of clouds to global warming, known as the "cloud feedback" over the Southern Ocean has been linked to higher levels of projected warming. To address the uncertainty, we apply a novel method to two satellite data sets. This method teases apart contributions from changing cloud properties such as their horizontal spatial coverage and their ability to reflect sunlight, to the cloud feedback, and then further dissects each of these contributions into those arising from changes occurring both within groups of cloud types and changes occurring between these groups. Results suggest that a general shift from thick storm-track clouds to thinner oceanic low-level clouds exacerbates warming in the Southern Ocean but are partially counterbalanced by cloud thickening in part due to stronger near-surface winds in the same region. Our novel methods and results can potentially be used to evaluate climate models and aid in tracing their shortcomings to poorly represented physical processes.

1. Introduction

The projected change in Earth's global mean surface air temperature is highly uncertain. In particular, the amount of warming to be expected due to a doubling of atmospheric CO_2 concentrations ranges from 2°C to 5°C with a probability greater than 90% based on multiple lines of evidence (Forster et al., 2021), including evidence based on global climate models (GCMs). The disparate response of clouds to global warming — referred to as the cloud feedback — continues to dominate the uncertainty in GCM-based climate projections for several decades (Forster et al., 2021). In fact, the most recent generation of GCMs participating in the sixth phase of the Climate Model Intercomparison Project (CMIP6) show enhanced warming relative to the previous generation of GCMs that

participated in the fifth phase of CMIP, that is, CMIP5 due to a 20% larger amplifying cloud feedback. Greater reductions in low-level cloud fraction (CF) and smaller increases in cloud water content, particularly over the Southern Ocean where mixed-phase clouds are abundant have been linked to the amplifying cloud feedback in GCMs participating in CMIP6 (Zelinka et al., 2020).

Yet, despite this uncertainty, robust features and a better physical understanding of cloud feedback mechanisms have emerged, in large part due to satellite observations. A wealth of data collected by spaceborne remote sensing instruments have contributed to constraining the cloud feedback either directly by inferring it from observations (Norris et al., 2016) or indirectly through improved representation and understanding of subgrid-scale processes that influence clouds (Coopman & Tan, 2023; Lebsock et al., 2013; Quaas, 2012; Soden & Donner, 1994; Su et al., 2013; Wang et al., 2022; M. H. Zhang et al., 2005; Z. Zhang et al., 2022) as well as through advances in understanding how local environmental factors control cloud properties (Kelleher & Grise, 2019; D. T. McCoy et al., 2020; Scott et al., 2020). The results presented herein are relevant to both approaches of constraining the cloud feedback: we apply satellite remote sensing observations directly to infer the interannual cloud feedback using a novel technique as a step toward indirectly improving GCMs at the process level. Although the interannual cloud feedback inferred from the novel technique employed here relates to short timescale processes that may not necessarily correspond to the long-term cloud feedback inferred from GCMs (Chao et al., 2024), many of the cloud processes that cause uncertainties in the long-term cloud feedback are observable short-term responses. Indeed, it has been shown that interannual and long-term cloud feedbacks are well-correlated across GCMs (Zhou et al., 2016). The technique applied here additionally diagnoses contributions of changing cloud morphology to the cloud feedback, which is missing from existing techniques.

The two main techniques that have been applied to diagnose cloud feedback are the partial radiative perturbation method (Wetherald & Manabe, 1988) and the "radiative kernel method." The latter method has diagnosed cloud feedback both directly through the development of the "cloud radiative kernel (CRK)" (Zelinka et al., 2012) as well as indirectly as a residual of the total climate feedback parameter (Shell et al., 2008; Soden et al., 2008). These methods do not diagnose the contributions due to changing cloud morphology, although a predictive model of certain cloud morphological changes has recently been developed (I. L. McCoy et al., 2023). Yet, at the same time, changes in cloud morphology have been shown to occur with global warming using the "cloud regime" framework (Tsushima et al., 2015; Williams & Tselioudis, 2007; Williams & Webb, 2009) that classifies clouds by dynamical regimes. *Cloud morphology* is used herein to broadly encompass cloud regimes that capture a mixture of traditional cloud types (Howard, 2011), although other definitions of cloud morphology exist in the literature (Stevens et al., 2019; Wood & Hartmann, 2006). The complementary strengths of the CRK and cloud regime concepts which were combined into a "double decomposition method" of the cloud feedback to diagnose the contribution of changing cloud morphology (Zelinka et al., 2023), are applied here to satellite observations to obtain the interannual cloud feedback. The method is applied to long-term satellite records of cloud properties obtained by the Moderate Resolution Imaging Spectroradiometer (MODIS) instrument onboard the Aqua and Terra satellites and archived in the International Satellite Cloud Climatology Project (ISCCP) data set.

The focus of this work is on the shortwave (SW) extratropical cloud optical depth feedback (λ_τ), that is, the contribution of changes in the optical depth (τ) of extratropical clouds to the SW radiation budget in response to rising global 2-m air temperatures holding cloud height and cloud amount fixed. A primary motivation behind this work is the cloud feedback over the Southern Ocean (defined as the latitude region spanning from 55°S to 65°S) since λ_τ in this region was shown to be a primary contributor to the increased projected warming in CMIP6 due to a weaker SW cloud scattering feedback in CMIP6 relative to CMIP5 (Zelinka et al., 2020). Several mechanisms have been proposed to explain the extratropical cloud feedback (D. T. McCoy et al., 2023). One reason for the weaker negative feedback is the increase in the proportion of supercooled liquid in mixed-phase clouds in the mean state of the CMIP6 models relative to that in the CMIP5 models (Bodas-Salcedo et al., 2019; Kawai et al., 2019; Zelinka et al., 2020). This increase in the mean-state liquid content of mixed-phase clouds implies that the transition from cloud ice to liquid water content at a given altitude is statistically less likely to occur — a mechanism referred to as the "cloud-phase feedback" (Frey & Kay, 2018; Mitchell et al., 1989; Tan et al., 2016; Tsushima et al., 2006; Wall et al., 2022). The cloud-phase feedback is a negative SW cloud feedback that acts to damp global warming. This is due to the fact that liquid droplets are more abundant than ice crystals in clouds (Pruppacher & Klett, 2012) coupled with the fact that clouds with a higher proportion of liquid water tend to be more reflective of sunlight than those with a higher

proportion of ice water (Sun & Shine, 1994). GCM simulations have shown that increasing the supercooled liquid water fraction of mixed-phase clouds causes the negative cloud-phase feedback to weaken (Tan et al., 2016). These simulations showed that as the cloud-phase feedback approaches the point of vanishing, it may unmask other warming mechanisms that contribute to a positive λ_τ. This effect was shown to be particularly prominent over the Southern Ocean due to an abundance of mixed-phase clouds (Haynes et al., 2011; Huang et al., 2012; Mace et al., 2021). Since the warming mechanisms contributing to a positive λ_τ are unknown, one of the main goals of this work is to determine how cloud morphological changes contribute to a positive λ_τ. Previous studies examining variations in satellite-observed τ with temperature at the cloud level suggest that decreases in τ with warming (Tan et al., 2019; Terai et al., 2016; Tselioudis et al., 1992) may indeed occur in the mid-latitude regions potentially due to increases in entrainment drying or precipitation with warming. In addition to thermodynamic phase shifts, increases in adiabatic liquid water content (Betts & Harshvardhan, 1987) and moisture convergence in the Southern Ocean and the subsequent increase in cloudiness and decrease in precipitation associated with it can also increase τ (D. T. McCoy et al., 2022). We apply the double decomposition method to elucidate how shifts in cloud morphology in response to changes in surface temperature warming contribute to λ_τ, with a focus on the Southern Ocean λ_τ.

We begin by describing the data sets used in this study in Section 2. The double decomposition method and the method for interpreting results are detailed in Section 3. Section 4 then presents the results of the application of the double decomposition method in the context of the interannual cloud feedback derived from two satellite remote sensing products. This is followed by concluding remarks in Section 5.

2. Data Sets

In this study, we employ the MODIS MCDCOSP joint histogram cloud product that merges cloud retrievals from both MODIS instruments onboard Terra and Aqua and is consistent with the satellite simulator framework (Pincus et al., 2023). We also repeat our analysis using the ISCCP High-resolution Global Hourly (HGG) joint histogram cloud product, and show these results in Supporting Information S1. We focus most of our discussion on MODIS because it uses more spectral information in its cloud property retrievals compared to ISCCP (Platnick et al., 2016; Young et al., 2018) and we therefore consider the MODIS retrievals to be relatively more reliable. In particular, while MODIS utilizes 22 out of its 36 spectral bands in its cloud mask algorithm (Ackerman et al., 2006; Platnick et al., 2016), ISCCP relies on two bands — one in the visible and the 11 μm infrared window band. MODIS retrieves τ using for the Nakajima and King (1990) bispectral method at 1 km pixel resolution; ISCCP infers τ using visible radiances and assuming thermodynamic phase from infrared radiances while making assumptions about the microphysical properties of the clouds.

There are key differences between MODIS and ISCCP that influence τ as highlighted in Pincus et al. (2012). These are briefly discussed here; the reader is referred to Pincus et al. (2012) for more details. First, the latter assumes that entire pixels are homogeneously cloudy whereas the former flags for partially cloudy pixels. Second, thermodynamic phase discrimination (which both products rely on to infer τ) differ; MODIS uses multiple spectral bands while ISCCP relies on a single threshold of brightness temperature. Third, the viewing and illumination geometry differ due to the fact that MODIS is polar-orbiting while ISCCP is a fusion of geostationary satellite data and polar-orbiting data, relying more heavily on geostationary data when available; while MODIS observations are concentrated near midday, ISCCP observations span all daytime hours and therefore include times when the solar zenith angle is low and therefore bias τ (Grosvenor & Wood, 2014). Fourth, the ISCCP data set contains a much greater proportion of optically thin cirrus clouds compared to MODIS and MODIS therefore generally exhibits a climatologically greater τ compared to ISCCP.

In this study, we employ the most up-to-date version of the ISCCP HGG weather states (Tselioudis et al., 2021a) and MODIS Collection 6.1 (Platnick et al., 2016) cloud regimes (Cho et al., 2021a). The centroids of the MODIS cloud regimes are displayed in Figure 1 and the global distributions of their relative frequency of occurrences are displayed in Figure 2. Briefly, MODIS cloud regimes 1–3 roughly correspond to tropical high-level clouds, cloud regime 4 to predominantly high-level subtropical clouds, cloud regimes 5–6 to high-latitude storm-track clouds, with cloud regime 6 predominantly occurring at mid-levels, and cloud regimes 7–11 corresponding to various low-level cloud types. The centroids of the ISCCP cloud regimes are displayed in Figure S1 and the global distributions of their relative frequency of occurrences are displayed in Figure S2. ISCCP cloud regime 1 roughly corresponds to tropical high-level clouds, 2 and 5 to high-latitude storm track clouds, 3 and 4 to cirrus clouds, and

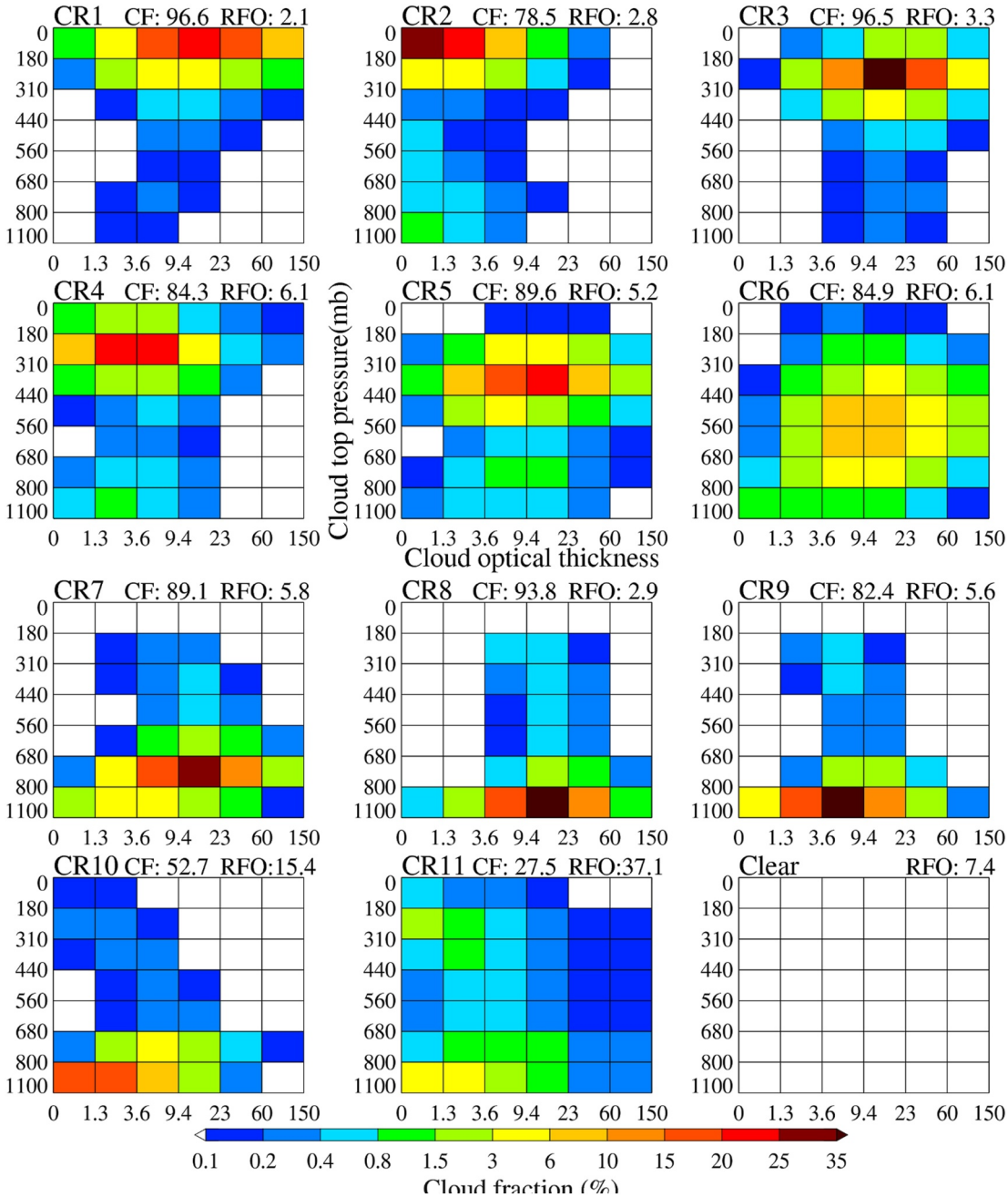

Figure 1. Global mean MODIS cloud regime centroids. The global relative frequency of occurrence and total cloud fraction of the cloud regimes are printed above each individual panel. These cloud regimes differ slightly from Cho et al. (2021a) in that they were derived from equal angle 1° daily joint-histograms as opposed to equal area (110 km)^2 3-hr joint histograms.

6–8 to various low-level cloud types. These descriptions are summarized in Table S1 in Supporting Information S1 and the reader is referred to the relevant publications for additional details on the derivation and description of the various cloud regimes.

Clear-sky surface albedo values were obtained using Edition 4.1 of the SYN Level 3 daily gridded observations of clear-sky surface albedo derived from the Clouds and the Earth's Radiant Energy System (CERES) instrument (Loeb et al., 2018). Global mean surface air temperature values, T_s are obtained from Modern-Era Retrospective analysis for Research and Applications, version 2 (MERRA-2) Reanalysis (Gelaro et al., 2017). The cloud-controlling factors examined in this study were also from MERRA-2 reanalysis.

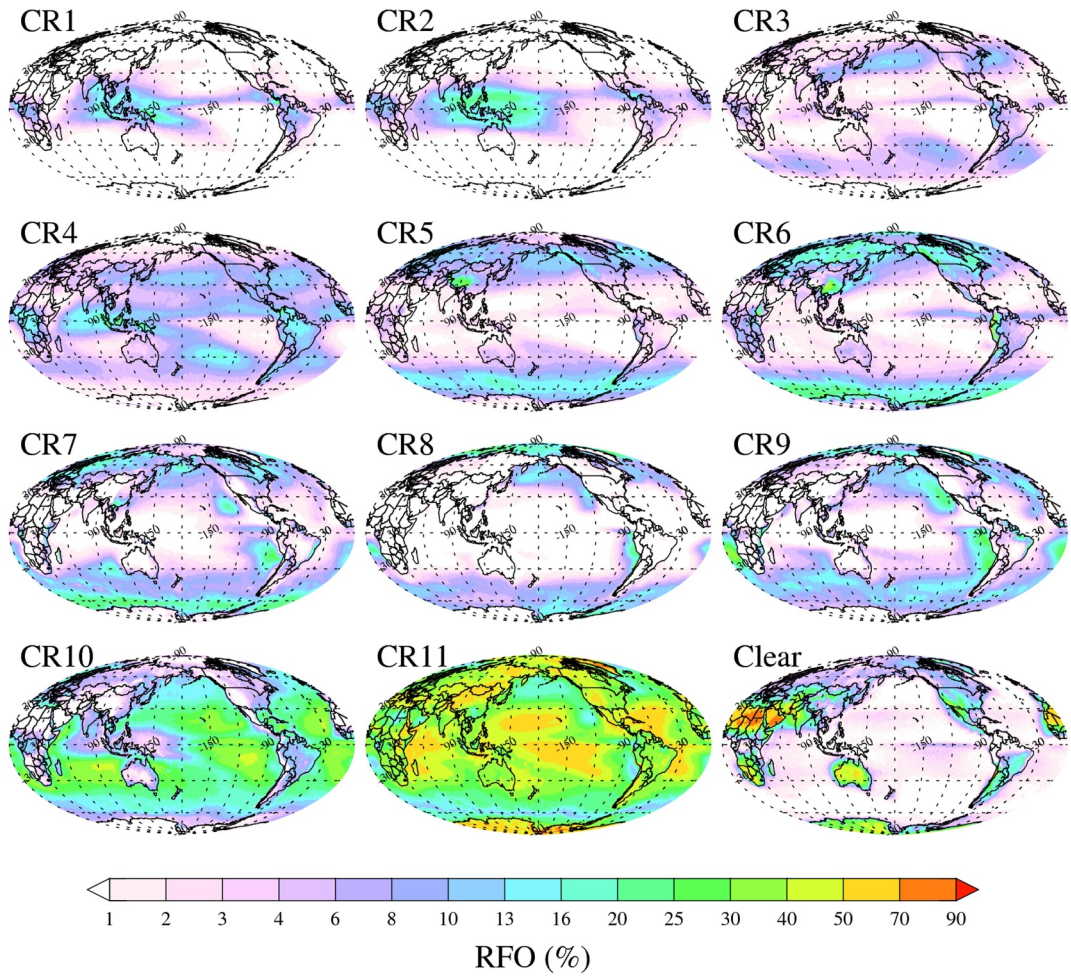

Figure 2. Global distributions of the relative frequency of occurrence of the MODIS cloud regimes.

3. Methodology

The principal method employed in this study — the double decomposition method — is described in Zelinka et al. (2023). A summary and modifications to this method (namely in the way anomalies were calculated and how the CRK was modified) are first described in Section 3.1. This method results in the decomposition of λ_τ, the cloud amount, and cloud altitude feedbacks into two dominant components: one that quantifies the contribution due to shifts between or "across" cloud regimes (described below) and another that quantifies the contribution of changes within cloud regimes to λ_τ. A method for interpreting the former component is detailed in Section 3.2.1 and the method employed to better understand the processes responsible for the latter component is detailed in Section 3.2.2.

3.1. Double Decomposition Method

The double decomposition method is a fusion of two independent techniques: the CRK decomposition technique (Zelinka et al., 2012, 2013) and the cloud regime decomposition technique (Williams & Tselioudis, 2007). The CRK method directly calculates the cloud feedback (with units of $\mathrm{Wm^{-2}K^{-1}}$) from cloud properties as the product of two terms:

$$\frac{dR}{dT_s} = \frac{\partial R}{\partial C}\frac{dC}{dT_s} \quad (1)$$

where R is the radiative flux at the top of the atmosphere and C is the CF joint-histogram. $K \equiv \frac{\partial R}{\partial C}$ is the CRK which is computed using an offline radiative transfer model and can essentially be considered a look-up table and $\frac{dC}{dT_s}$ is the sensitivity of the *monthly* CF to changes in T_s. The CRK term is a five-dimensional matrix consisting of τ, cloud top-pressure, latitude, albedo, and month. The CRK is quantified and stored separately for both longwave and SW radiation components. As described in Zelinka et al. (2012), the SW CRK replaces longitude with three values of albedo to account for the fact that changes in SW radiation due to clouds also depends on the underlying surface albedo. The matrix convention used in the CRK method derives from the ISCCP joint-histogram framework that records the presence of cloudy pixels in various ranges or "bins" of τ and cloud-top pressure within a given grid cell. The total cloud feedback, λ_{tot} can be decomposed into components due to changes in cloud amount, pressure, and optical depth, plus a residual term, in each case holding the other properties fixed, that is,

$$\lambda_{tot} = \lambda_\tau + \lambda_a + \lambda_p + \lambda_r \tag{2}$$

where the subscripts "a," "p," and "r" represent amount, pressure, and residual, respectively. Equations for these terms are provided in Appendix B of Zelinka et al. (2013).

The advent of the satellite simulator (Bodas-Salcedo et al., 2011) has effectively enabled a relatively fair comparison and therefore evaluations of GCM-simulated cloud properties against satellite observations. Cloud histograms can be obtained either from models and/or observations and are also five-dimensional matrices. Cloud regimes are a mixture of traditional cloud types (Howard, 2011) derived by applying the k-means clustering algorithm (Anderberg, 1973) on gridded cloud histograms. A set of histograms with substantially different cloud properties is determined to initialize the clustering algorithm. The result after convergence of the algorithm is a set of centroids representing cloud properties with distinct thermodynamical and dynamical meteorological regimes (Oreopoulos et al., 2014). The cloud regime concept was originally applied to ISCCP cloud histograms at a *3-hr temporal resolution* (Jakob & Tselioudis, 2003) and later extended to *daily* MODIS cloud histograms (Oreopoulos et al., 2014). Individual grid cells can then be assigned to individual cloud regimes. For example, for MODIS cloud regimes that are defined in 1° grid cells on a daily basis, each grid cell is labeled as one of cloud regimes 1–11 (or the clear-sky regime 12) determined to be the cloud regime with the centroid that has the smallest Euclidian distance from the histogram of the grid cell. For simplicity, the term "cloud regime" is henceforth a generic term we will use to include ISCCP cloud regimes that were originally coined "weather states" in addition to MODIS cloud regimes. The concept of cloud regimes has been particularly useful for application to GCMs by virtue of their classification on the gridded spatial scale which makes them compatible for evaluation against satellite observations (Tsushima et al., 2015; Williams & Webb, 2009).

The basic idea of fusing together the CRK and cloud regime decomposition techniques is to insert a cloud regime-decomposed CF anomaly into Equation 1. Given that the CRK has a temporal resolution of 1 month, we define the cloud regime-decomposed CF anomaly to be a monthly anomaly to be compatible with the CRK. The monthly cloud anomaly, ΔC can be decomposed as follows:

$$\Delta C = \sum_{r=1}^{N} \left(\Delta f_r C_r + \Delta C_r f_r + \Delta C \Delta f_r \right), \tag{3}$$

where N represents the total number of cloud regimes (there are a total of 8 and 11 cloud regimes for ISCCP and MODIS, respectively), and f_r represents the RFO of a cloud regime within a given period of time — here, taken to be a month to be compatible with the CRK method. Therefore,

$$f_r(m, \phi, \theta) = \frac{\sum_{y=y_i}^{y_f} \sum_{d=1}^{D(m_y)} n_r(d, \phi, \theta)}{\sum_{r=1}^{R} \sum_{y=y_i}^{y_f} \sum_{d=1}^{D(m_y)} n_r(d, \phi, \theta)}, \tag{4}$$

where y denotes the year, m is the month, D denotes the total number of days in a given month, ϕ is the longitude coordinate and θ is the latitude coordinate and n_r is the occurrence of a cloud regime in each day and at each location, and n is a boolean value. Here, a cloud regime's monthly cloud anomaly, ΔC_r is defined as the difference

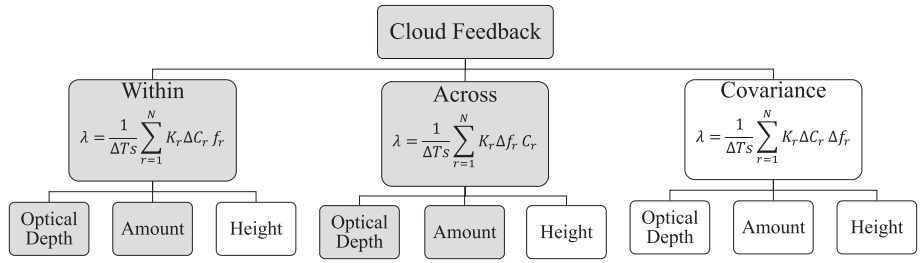

Figure 3. Flowchart illustrating the double decomposition of the shortwave (SW) cloud feedback and the associated terminology. The gray-boxes represent the non-negligible SW cloud feedbacks presented in this manuscript. The residual term of the cloud radiative kernel method is not shown for simplicity. Note that within each of the three rows, each term is the sum of 11 cloud regimes or 8 weather states for MODIS and International Satellite Cloud Climatology Project, respectively.

between the regime's CF at a particular month and the cloud regime's climatological monthly mean over the time period of interest C_r. In this case, the time period of interest is from 2003 to 2016. This time period is limited by the availability of the MODIS cloud regimes post-2003 and ISCCP weather states pre-2016. The first term on the right-hand side of Equation 3 represents the contribution of shifts in the RFO of a particular cloud regime to ΔC (henceforth referred to as the "across-regime term"); the second term represents the contribution of changes due to properties within a particular cloud regime to ΔC (henceforth referred to as the "within-regime term") and the third term represents the contribution of both across-regime shifts and within-regime changes in cloud properties (henceforth referred to as the "covariance term").

The CRK and cloud regime decomposition methods can be fused together by substituting ΔC in Equation 3 into Equation 1 to obtain the total cloud feedback parameter, λ_c:

$$\lambda_c = \frac{1}{\Delta T_s}\sum_{r=1}^{N} K_r\left(\Delta f_r C_r + \Delta C_r f_r + \Delta C \Delta f_r\right) \tag{5}$$

The normalization by ΔT_s is performed by regressing monthly mean cloud-induced radiation anomalies, ΔR (the terms in the summation) onto monthly global mean ΔT_s values. K_r (which is different for the ISCCP and MODIS cloud regimes) represents the CRK corresponding to a given cloud regime. The SW K_r was derived by first creating a clear-sky surface albedo weighted by the frequency of occurrence of each cloud regime for each latitude. These monthly derived surface albedo values are then used to map via linear interpolation the SW K_r to longitude coordinates for each cloud regime. The decomposition represented by Equation 5 is referred to as the "double decomposition method" and is so-called because it reflects the fact that it decomposes λ_c into three components plus a residual term following the standard CRK technique and then each of those components into another three components following the cloud regime decomposition method. The double decomposition method is schematically represented by the three rows in Figure 3.

The contribution of the across-regime term to cloud optical depth and altitude feedback vanishes by design. This arises from the fact that it consists of a product of a scalar, Δf_r and two mean-state variables, C_r and K_r. Yet, across-regime changes that occur when cloud property changes are large enough to result in a regime shift may represent substantial contributions to these cloud feedbacks as later shown in Section 4. Thus, following Zelinka et al. (2023), the first term on the right-hand side of Equation 5 is further decomposed as

$$K_r \Delta f_r C_r = \Delta f_r\left(\overline{CK} + \overline{C}K'_r + C'_r\overline{K} + C'_r K'_r\right), \tag{6}$$

where the overbar denotes the annual and cloud regime average, and the prime denotes the anomaly from that average. The sum of the first term, $\Delta f_r \overline{CK}$ over all cloud regimes vanishes since the change in CF across cloud regimes is conserved. Also, by design, the change in CF across cloud regimes is large in comparison to changes in the CRK itself across cloud regimes. Therefore the second and fourth terms, $\Delta f_r \overline{C}K'_r$ and $\Delta f_r C'_r K'_r$, respectively, are small in comparison with the third term, $\Delta f_r C'_r \overline{K}$, which represents the component due to

Table 1
Average Cloud Fraction-Weighted τ Over the Southern Ocean (55°S to 65°S) for the MODIS Cloud Regimes for Years 2003–2020

Cloud regime number	Average τ
1	20.6
2	7.7
3	19.4
4	10.8
5	16.5
6	18.8
7	19.7
8	18.3
9	10.7
10	8.1
11	13.7

changes in the RFO of each regime multiplied by the deviation of climatological cloud properties from their annual- and regime-mean values (which we simply refer to as the perturbation term denoted by the prime). This third term is the dominant term in Equation 6. Therefore, the final equation for cloud feedback calculated herein is

$$\lambda_c \approx \frac{1}{\Delta T_s}\sum_{r=1}^{R}\left(\Delta f_r C_r' \overline{K} + K_r\left(\Delta C_r f_r + \Delta C \Delta f_r\right)\right) \quad (7)$$

We refer to calculations of the cloud feedback that do not involve cloud regimes as the "non-CR-decomposed" cloud feedback in contrast to the "double-decomposed" cloud feedback in Equation 7. Sources of uncertainty in the calculation of the SW λ_τ through this methodology include assumptions about the CRK including fixed particle sizes for liquid and ice hydrometeors, the relatively coarse binning of the CRK itself, the atmospheric input data assumed in radiative transfer model used to develop the CRK, and the linearity assumption in the CRK method itself. The usage of both MODIS and ISCCP attempts to address uncertainty in C and f.

A few caveats regarding the interpretation of the across-regime contribution to λ_τ are worth noting. First, in the case where multiple cloud regimes are associated with across-regime shifts, it is not possible to unambiguously determine the detailed type of shifts of specific cloud types and where the clouds are shifting to and from. Rather, we can only check for consistency between MODIS and ISCCP observations, and as previously shown, there are several instances where the two data sets disagree. For example, in the case of cloud regime shifts contributing to negative values of λ_τ over the Southern Ocean, both MODIS and ISCCP show that the feedback arises from shifts from thin, low-level omnipresent clouds to thick storm-track clouds (Table 2). The contribution to positive values of λ_τ over the Southern Ocean, where there is an unambiguous shift from thick mid-level clouds toward relatively thinner lower-level clouds is robustly observed with both ISCCP and MODIS observations. However, the specific cloud types involved cannot be unambiguously determined.

3.2. Interpretation Methods

The results from the double decomposition method can be paired with additional information to gain further insight into mechanisms associated with λ_τ, which is the focus of this study. Since the covariance term is negligibly small in comparison (Figures S3 and S4 in Supporting Information S1), the additional information we use to interpret the results is only paired with the across-regime and within-regime components of λ_τ.

Table 2
Summary of Dominant Across-Regime Shifts Contributing to λ_τ Following the Interpretation Method Illustrated in Figure 4 and Broken Down Into Contributions Resulting in Positive and Negative Values for the Upper and Lower Southern Ocean

Contributions from Cloud Regimes		Total Feedback
$f_r < 0$ (from thicker)	$f_r > 0$ (to thinner)	
Upper Southern Ocean (55˚S to 60˚S)		
1, 2, 5	7, 8, 9	Positive
Thick, storm-track and deep convective	Thinner, stratocumulus	
Lower Southern Ocean (60˚S to 65˚S)		
$f_r < 0$ (from thinner)	$f_r > 0$ (to thicker)	
11	3, 5	Negative
Thin, low-level, omnipresent	Thick storm-track clouds	

Note. Cloud regime indices refer to MODIS cloud regimes.

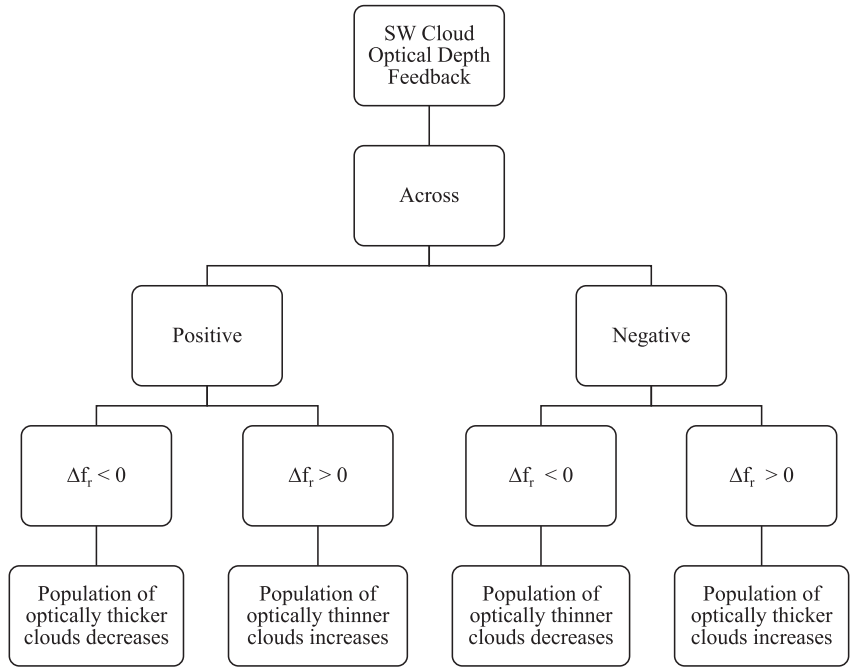

Figure 4. Illustration of the method for interpreting the across-regime component of the shortwave λ_τ assuming that $\Delta T_s > 0$.

3.2.1. Across-Regime Interpretation

The across-regime contribution to λ_c or any one of its three components for a given cloud regime is mathematically represented by the term $\frac{1}{\Delta T_s}\overline{K}\Delta f_r C'_r$. Physically, this term represents the shift from one cloud regime to another. Given this term alone, it is not possible to track where cloud regimes are shifting to and from. However, pairing information about the sign and magnitude of the term with concurrent changes in the frequency of occurrence of cloud regimes in response to changes in ΔT_s can reveal relevant information.

The procedure for this method is displayed in Figure 4 for the SW λ_τ of interest in this study. This is illustrated by the left-hand branch of Figure 4. The converse interpretation holds true if the across-regime contribution to λ_τ is negative (illustrated by the right-hand branch of Figure 4).

3.2.2. Within-Regime Interpretation

The within-regime contribution to λ_c or any one of its three components for a given cloud regime is mathematically represented by the term $\frac{1}{\Delta T_s}K_r\Delta C_r f_r$. Physically, this term represents changes in cloud properties that occur within a given cloud regime. This includes any change within the cloud regime itself that is not substantial enough to cause a shift to another cloud regime. In the latter case where the change in the cloud regime is sufficient to cause shift to another cloud regime, we refer to this as an across-regime shift. To provide a physical understanding of what drives within-regime contributions to λ_τ, a multiple linear regression analysis using a common method in the literature is performed to explain changes in cloud optical depth, and this information is paired with the results of the double decomposition method. In particular, for a multiple linear regression analysis where the response variable is monthly average grid-mean CF-weighted ln τ of a particular cloud regime and the explanatory variables are monthly gridded-mean averages of meteorological factors that impact τ, known as "cloud-controlling factors," x_i (Klein et al., 2017; Stevens & Brenguier, 2009), the coefficients of the multiple linear regression, $\frac{\partial \ln \tau}{\partial x_i}$ yield the sensitivity of low-level CF-weighted ln τ to the cloud-controlling factors. Low-level clouds are of particular interest as they may react more quickly to local environmental parameters which may thus modulate the long-term response of these clouds (Klein et al., 2017). The product of these coefficients with the total derivative of the cloud-controlling factor with respect to global surface air temperature, T_s, that is, $\frac{\partial \ln \tau}{\partial x_i}\frac{dx_i}{dT_s} = \frac{d \ln \tau}{dT_s}$ represents the contribution of the cloud-controlling factor to the change in logarithmic cloud optical depth in response to a change in global surface air temperature. Cloud

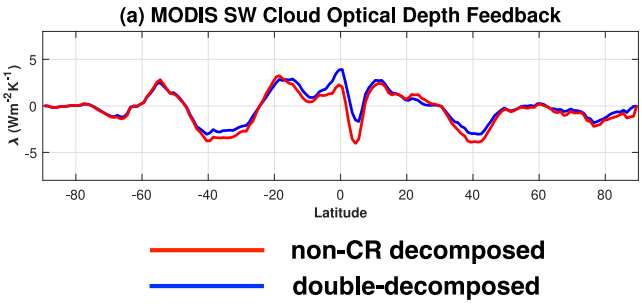

Figure 5. Zonal averages of shortwave λ_τ inferred from MODIS and computed as the total non-CR decomposed feedback (red) and the double-decomposed cloud feedback (blue).

controlling-factor analysis has been previously employed to reveal insight into physical mechanisms responsible for cloud feedback via CF changes (Kelleher & Grise, 2019; D. T. McCoy et al., 2020; Scott et al., 2020; Terai et al., 2016).

The cloud-controlling factors include the estimated inversion strength (EIS) (Wood & Bretherton, 2006), the updraft velocity at 700 hPa (ω_{700}), the relative humidity at 700 hPa (RH_{700}), temperature advection (T_{adv}), sea-surface temperature (T_s) and the wind speed at 2 m above the surface (WS). EIS is defined as

$$EIS = LTS - \Gamma_m^{850}(Z_{700} - Z_{LCL}), \tag{8}$$

where LTS is the lower-tropospheric stability, taken to be the difference in potential temperature between 700 hPa and the surface, Γ_m^{850} is the moist adiabatic lapse rate at 850 hPa, Z_{700} is the height above the surface corresponding to the 700 hPa pressure level, and Z_{LCL} is the height above the surface of the lifting condensation level. T_{adv} is defined as

$$T_{adv} = -\frac{U_{10}}{R_E \cos\theta}\frac{\partial T_s}{\partial \phi} - \frac{V_{10}}{R_E}\frac{\partial T_s}{\partial \theta}, \tag{9}$$

where U_{10} is the zonal wind component at 10-m above the surface and V_{10} is the meridional wind component at 10-m above the surface. Note that negative values of T_{adv} indicate cold air advection and positive values indicate warm air advection. To put the roles of the various cloud-controlling factors on equal footing, each is normalized by one local standard deviation anomaly.

The multiple linear regression analysis was performed separately for each cloud regime for the same time period used for the double decomposition method. The fact that each grid cell in a single day is classified as a single cloud regime limits the amount of data available for certain cloud regimes in a particular region. Thus, CF-weighted ln τ and cloud-controlling factors were first extracted for each cloud regime and averaged over the Southern Ocean before performing the multiple linear regression analysis for each cloud regime.

4. Results

The double-decomposed SW λ_c derived using both MODIS and ISCCP observations and the interpretation of these results are presented in this section. For the sake of brevity, we present the majority of the ISCCP results in the Supporting Information section. The components of λ_c presented herein are shaded in gray in Figure 3. While the longwave component of λ_c can be similarly analyzed and decomposed, the results are not presented here for the sake of simplicity. Since the cloud height component of λ_c and the covariance term of the double decomposition method are negligibly small compared to the other feedbacks, they are not shown.

4.1. Zonal Averages of Cloud Feedbacks

We begin by presenting zonal averages of the non-CR decomposed interannual λ_τ computed using MODIS observations (Figure 5). The non-CR decomposed interannual cloud amount feedback derived from MODIS is displayed in Figure S5 in Supporting Information S1. The ISCCP-calculated values for both λ_τ and the cloud amount feedback are presented in Figure S6 in Supporting Information S1. MODIS shows a more positive λ_τ over the "upper" Southern Ocean (defined here as the region extending from 55°S to 60°S) compared to ISCCP while MODIS shows a somewhat comparable value in the "lower" Southern Ocean (defined here as the region extending from 60°S to 65°S). Negative values also occur over the Southern Hemisphere (SH) subtropical latitudes, and positive values occur in the SH tropics. Although these observation-derived λ_τ values are representative of the interannual feedback, there is evidence that the feedback is timescale invariant and therefore representative of the long-term λ_τ derived from GCMs (Terai et al., 2016). In contrast, ISCCP shows a more muted negative λ_τ over the Southern Ocean and a more muted positive value over the Northern Hemisphere (NH) subtropical regions than MODIS. The ISCCP-derived λ_τ and cloud amount feedback are generally smaller in magnitude compared to that of MODIS for all latitudes.

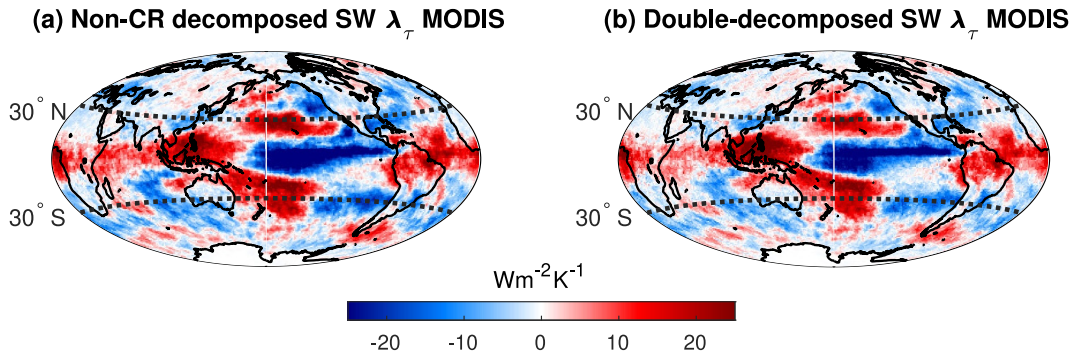

Figure 6. Global distributions of the MODIS-derived shortwave (a) non-CR decomposed cloud optical depth feedback and (b) double-decomposed cloud optical depth feedback.

Next, we demonstrate the effectiveness of the double decomposition method in reproducing λ_τ derived without involving cloud regimes by summing the components of the feedback (Figure 5). Figure 5 shows that the summation of the double-decomposed feedback components (where λ_τ includes the additional term $\Delta f_r C_t \overline{K}$ in Equation 7) are generally able to capture the non-CR decomposed cloud optical depth feedback. Global distributions of these feedbacks (Figure 6 and Figure S5 in Supporting Information S1) show that patterns are generally consistent. The largest discrepancies using the ISCCP data set occur over the Antarctic continent (Figures S6 and S7 in Supporting Information S1). The discrepancies between the two calculations can be attributed to both the remaining nondominant terms not included in the calculation in Equation 6 and the nonlinearity of the CRK decomposition method. We caution that passive retrievals for identifying cloudy pixels are not reliable in the polar regions (approximately poleward of 65° latitude) due to the lack of thermal contrast over bright surfaces (Chan & Comiso, 2013; Liu et al., 2010) and three-dimensional radiative effects particularly at large solar zenith angles (Grosvenor & Wood, 2014) can influence retrievals of cloud properties.

4.2. Southern Ocean Distributions of Cloud Feedbacks

Southern Ocean distributions of the non-CR decomposed interannual λ_τ and cloud amount feedback are displayed in Figure 7 and Figure S8 in Supporting Information S1, respectively for MODIS-derived values. Their counterparts for ISCCP are shown in Figure S9 in Supporting Information S1. Consistent with the zonal averages displayed in Figure 5, the magnitude of the MODIS cloud feedback values are generally larger regionally.

The contributions of the cloud amount feedback dominate the total cloud feedback (Figure 7 and Figure S8 in Supporting Information S1). MODIS shows that both the cloud amount and cloud optical depth feedback

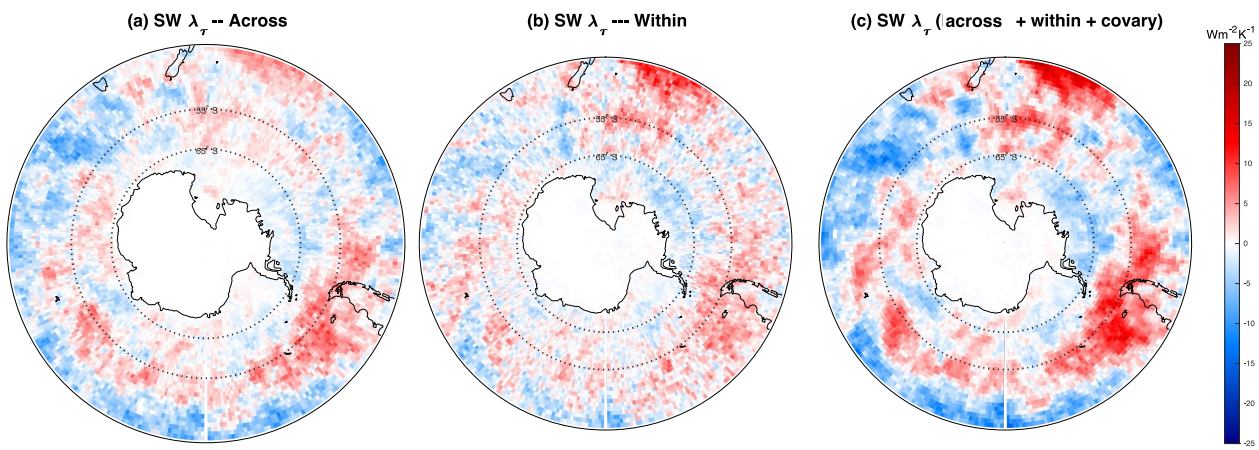

Figure 7. Southern Ocean MODIS-derived shortwave (a) across-regime, (b) within-regime, and (c) total (including the cloud height feedback) λ_τ. Each panel represents the sum of all cloud regimes.

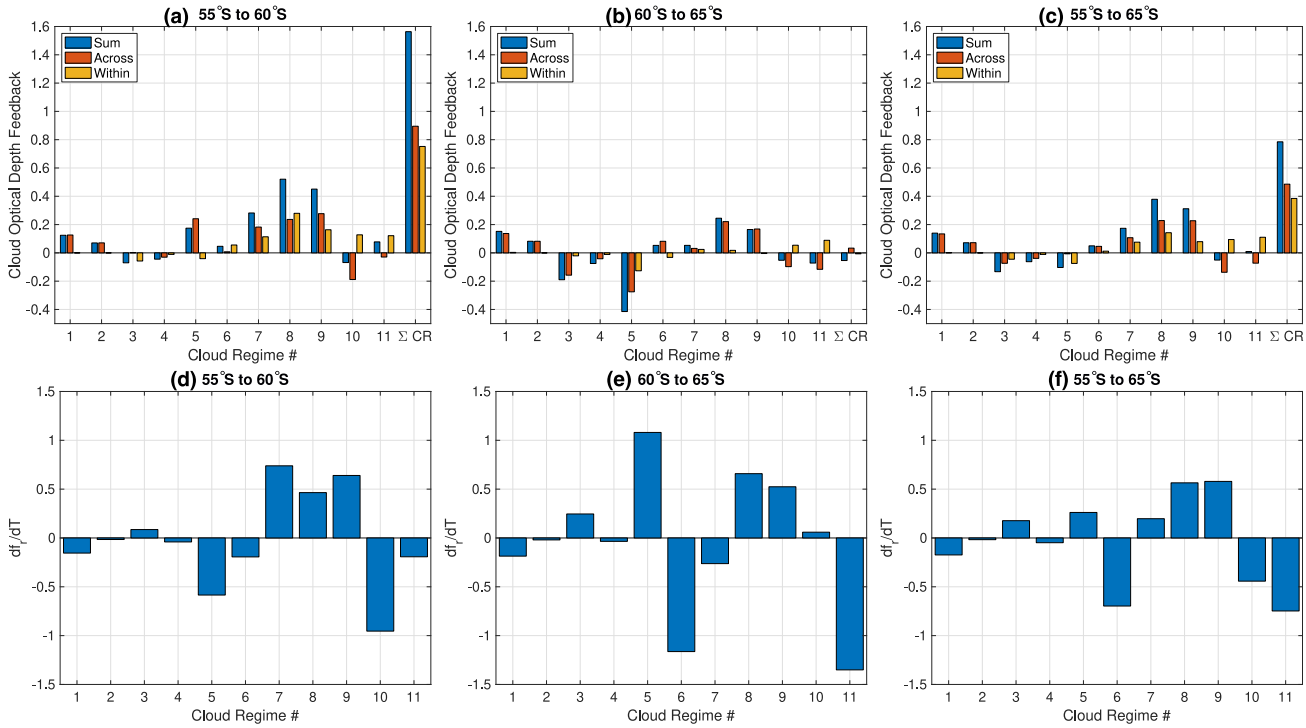

Figure 8. Average MODIS-derived double-decomposed shortwave cloud optical depth feedback over the Southern Ocean decomposed into cloud regime contributions over the (a) upper Southern Ocean, (b) lower Southern Ocean, and (c) greater Southern Ocean including the upper and lower Southern Ocean. Change in the f_r of each MODIS CR in response to global mean surface air temperature in units of percent per degree K decomposed into cloud regime contributions over the (d) upper Southern Ocean, (e) lower Southern Ocean, and (f) greater Southern Ocean including the upper and lower Southern Ocean.

components contribute similarly to the within-regime feedback. ISCCP shares both these features (Figure S9 in Supporting Information S1).

When comparing the across- and within-regime contributions, the across-regime contribution is somewhat weaker but comparable to the within-regime contribution to λ_τ for both MODIS and ISCCP (Figure 7 and Figure S9 in Supporting Information S1). However, the across-regime contribution is clearly larger than the within-regime contribution for the cloud amount feedback in the ISCCP data set (Figure S9 in Supporting Information S1).

Contrasting MODIS and ISCCP in Figure 7 and Figure S9 in Supporting Information S1, the sign of the decomposed feedback components are in agreement in some regions between the two data sets. The location of the positive and negative across-regime contributions to λ_τ (Figure 7a and Figure S9g in Supporting Information S1) are in better agreement than that for the within-regime contribution (Figure 7b and Figure S9h in Supporting Information S1). Overall, each of the ISCCP decomposed feedback components is generally smaller in magnitude compared to those of MODIS.

4.3. Across-Regime Interpretation

Following the method of interpreting the across-regime contribution to λ_τ described in Section 3.2.1, we now present the results of this method. From Figure 5, the MODIS λ_τ is positive in the region extending from 55°S to 60°S and negative in the region extending from 60°S to 65°S. Our analysis over the Southern Ocean will therefore be separated into the upper and lower Southern Ocean.

Here, we use both the average double-decomposed cloud feedback contributions of the individual cloud regimes over the Southern Ocean as well as the average changes in f_r over the Southern Ocean for each cloud regime in

response to ΔT_s displayed in Figure 8 and Figure S10 in Supporting Information S1 for MODIS and ISCCP, respectively, for our interpretation.

Figure 8a shows the overall positive λ_τ due to across-regime shifts in the upper Southern Ocean derives from cloud regimes 1, 2, 5, 7, 8, and 9 (left hand side branch of Figure 4). MODIS cloud regimes 1 and 2 are dominated by tropical deep convective clouds with rare occurrences in the Southern Ocean region (Cho et al., 2021a). Cloud regime 5 is dominated by oceanic storm-track clouds. Cloud regime 7 is commonly found in the mid-latitudes and contains mid-level but even more low-level clouds. Cloud regimes 8 and 9 are a combination of frequently occurring low-level stratocumulus and stratus clouds. Of these cloud regimes, Figure 8d shows that cloud regimes 7, 8, and 9 increase in their RFO with ΔT_s (fourth row, second to leftmost branch of Figure 4). Although cloud regimes 7 and 8 are optically thicker on average compared to the other cloud regimes, they do contain a sizable population of optically thin clouds whose frequency of occurrences are not quantified in this analysis. The largest contribution is due to cloud regime 9 which has an average CF-weighted τ of 10.7 over the Southern Ocean (Table 1) — a value that is smaller than the simple arithmetic average across all cloud regimes. At the same time, decreases in the frequency of occurrences of cloud regimes 1, 2, and 5 occur (fourth row, leftmost branch of Figure 4). The most negative Δf is due to cloud regime 5 which has an average CF-weighted τ of 16.5 (Table 1), which is slightly above the simple arithmetic average across all cloud regimes. Therefore, although the populations of several cloud regimes change and contribute to a positive λ_τ, the largest contributors are decreases in the population of optically thick oceanic storm-track clouds (cloud regimes 5) and increases in the population of the portion of optically thinner stratocumulus clouds that occur within cloud regimes 7–9 but primarily cloud regime 9 in the Southern Ocean (Figure 4 bottom row, left two branches).

Applying this same procedure to understand the overall small negative λ_τ value in the lower Southern Ocean shows that cloud regimes 3, 4, 5, 10, and 11 are the primary contributors to the negative feedback (Figure 8b). Cloud regimes 3, 5, and 10 increase in their RFO with ΔT_s, with cloud regime 5 being the dominant contributor to the negative feedback (Figure 8e). Cloud regime 4 and especially 11 decrease in their RFO although the contribution due to cloud regime 4 is negligible. The strong increase in cloud regime 5, which has an average CF-weighted τ of 16.5, and the decrease in omnipresent cloud regime 11, which has an average CF-weighted τ of 13.7, causes the overall cloud optical depth feedback to be slightly negative in the lower Southern Ocean. Therefore, oceanic storm-track clouds represented by cloud regime 5 play an active role in the Southern Ocean, contributing to a positive feedback in the upper Southern Ocean but a negative feedback in the lower Southern Ocean. Overall, the cloud optical depth feedback over the Southern Ocean (55°S to 65° S) is slightly positive primarily due to stratocumulus-dominated cloud regimes 8 and 9 (Figures 8c and 8f).

An analogous procedure for ISCCP observations (Figure S10 in Supporting Information S1) reveals consistency with the MODIS observations: the upper and lower Southern Ocean show a dominant positive and negative across-regime contribution to λ_τ, respectively, however ISCCP shows an overall negative λ_τ. In the upper Southern Ocean, ISCCP consistently shows that decreases in optically thick high-level clouds (cloud regime 2) contribute to a positive value of λ_τ and also that storm track clouds (cloud regime 5) and stratocumulus clouds (cloud regime 8) contribute to a positive λ_τ in the region. However, ISCCP shows a smaller role due to storm track clouds compared to MODIS. In the lower Southern Ocean, ISCCP also consistently shows that an increase in optically thick storm-track clouds and a decrease in omnipresent fairweather cumulus clouds contribute to a negative λ_τ. ISCCP however, does show several other contributors to the negative λ_τ, including contributions from shallow cumulus clouds, stratocumulus clouds and cirrus clouds. These results are summarized in Table 2.

4.4. Within-Regime Interpretation

We focus our analysis over the Southern Ocean due to its aforementioned importance in the enhanced projected warming in the CMIP6 models. Furthermore, because the influence of mostly near-surface meteorological parameters is likely to influence low-level cloud properties, we further restrict the regression analysis to MODIS cloud regimes 5 to 11, noting that cloud regimes 5 and 6 also contain a substantial amount of mid-level clouds (i.e., those with cloud top pressure between 680 and 440 hPa). The coefficients of the multiple linear regression analysis representing the sensitivity of MODIS-retrieved CF-weighted ln τ in response to a one-standard deviation change in the six cloud-controlling factors (while holding the others constant) are displayed in Figure 9a. The r^2 values for the multiple linear regression method, indicating the ability of the model

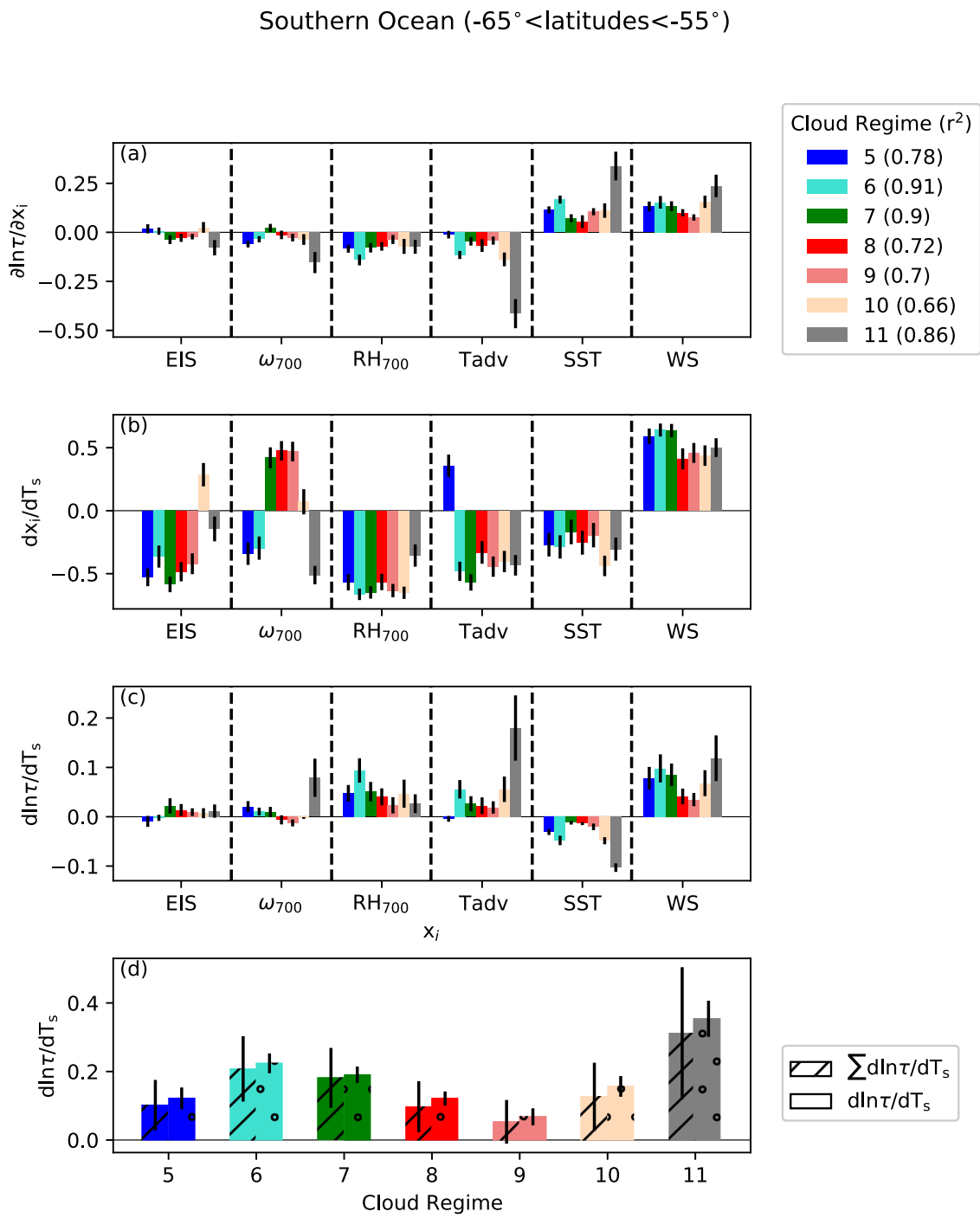

Figure 9. (a) Coefficients of the multiple linear regression analysis over the Southern Ocean described in Section 3.2.2. Each coefficient quantifies the response of the MODIS CF-weighted logarithm of cloud optical depth to a change in one standard deviation of an individual cloud-controlling factor, x_i while holding all other x_i constant. (b) Total derivative of the change in each cloud-controlling factor with respect to a change in global mean surface temperature change. (c) Change in the CF-weighted logarithm of cloud optical depth in response to global mean surface temperature changes attributed to each cloud-controlling factor. (d) Sum of the surface temperature-induced changes in CF-weighted cloud optical depth due to the cloud-controlling factors, $\frac{d \ln \tau}{dT_s}$ for each cloud regime (bars with diagonal stripes) and $\frac{d \ln \tau}{dT_s}$ computed independent of cloud-controlling factors (dotted bars). The MODIS cloud regimes are color-coded and labeled in the legend. r^2 for the multiple linear regression analyses are displayed in brackets. Error bars represent two standard deviations in the regression.

to explain the variance in ln τ and therefore reproduce the observations for cloud regimes 5–11 are also displayed in the legend of Figure 9. Figure 9b shows the sensitivity of the individual cloud-controlling factors to the change in the global mean surface temperature, and Figure 9c shows the product of Figures 9a and 9b for each individual cloud-controlling factor and MODIS cloud regime. The sum of contributions to the surface temperature-induced changes in CF-weighted ln τ due to all cloud-controlling factors for each cloud regime are displayed in Figure 9d.

It is important to note that the coefficients express changes in ln τ to changes in each of the cloud-controlling factors; there is no link made to changes in the top-of-the-atmosphere SW radiation budget, which is the quantity directly linked to the cloud feedback. Therefore, a positive coefficient indicates that an increase in the magnitude of the cloud-controlling factor results in an increase in ln τ. Increasing ln τ increases the albedo of clouds with respect to sunlight roughly linearly, and therefore increases the amount of SW radiation returning back to space at the top of the atmosphere. Conversely, a negative coefficient indicates that the cloud-controlling factor reduces ln τ.

We start by discussing the role of EIS, which has been shown to be an important cloud-controlling factor of CF in the Southern Ocean (Naud et al., 2023). While EIS is associated with increases in ln τ for some cloud regimes, it also decreases ln τ for other cloud regimes (Figure 9a). By definition, the EIS is a measure of the strength of the capping temperature inversion above cloud top. The role of EIS in ln τ depends on the moisture levels of the free-troposphere: a weaker EIS in a moister free-troposphere would increase ln τ and therefore result in a negative $\frac{\partial \ln \tau}{\partial EIS}$ coefficient, whereas a weaker EIS in a drier free-troposphere would decrease ln τ and therefore result in a positive $\frac{\partial \ln \tau}{\partial EIS}$ coefficient. Therefore, the cloud regimes associated with negative $\frac{\partial \ln \tau}{\partial EIS}$ coefficients may be present in regions of weak stability with a moister free troposphere. When the multiple linear regression analysis is repeated at the higher latitudes of 60°S to 70°S, ln τ consistently increases with EIS (Figure S11 in Supporting Information S1). This suggests that EIS at higher latitudes, where the atmosphere tends to increase in its thermodynamic stability, acts to trap moisture in the boundary layer, which is conducive to low-level cloud formation and enhancing the water content and hence optical thickness of the clouds. These results at higher latitudes are consistent with Terai et al. (2016) who also found positive coefficients derived from a suite of satellite observations over both the NH and SH which were taken to extend between 40°S and 70°S latitude in their respective hemispheres. Referring back to the analysis over 55°S to 65°S displayed in Figure 9, EIS in the low-level cloud regime regions over the Southern Ocean quite consistently decreases with global surface temperature warming (Figure 9b) and the overall effect of EIS is to cause an increase in ln τ with warming (Figure 9c).

Increases in subsidence strength generally serve to decrease ln τ. Figure 9a shows that this is the case for nearly all cloud regimes with one exception. It is notable that the coefficient is large in magnitude for MODIS cloud regime 11, indicating the strong influence of downdraft velocity on these omnipresent mixtures of cloud types. Unlike the sensitivity of ln τ to downdraft strength, the sign of the change in downdraft strength with global surface temperature warming is not consistent across cloud regimes (Figure 9b). The net effect of downdraft strength is to increase ln τ with global surface air temperature for most cloud regimes but decrease it for others (Figure 9c).

The impact of decreasing RH_{700} is to increase ln τ as indicated by the negative $\frac{\partial \ln \tau}{\partial RH_{700}}$ coefficients for most cloud regimes (Figure 9a). We speculate that the negative $\frac{\partial \ln \tau}{\partial RH_{700}}$ coefficients may be caused by reductions in downwelling longwave radiation from water vapor and/or upper-level clouds overlying low-level clouds that increase cloud top radiative cooling and therefore turbulent circulations that couple the cloud layer to the moist surface that are conducive to formation (Christensen et al., 2013). RH_{700} consistently decreases with global mean surface warming (Figure 9b). As a result, RH_{700} is associated with a net decrease in ln τ as global surface air temperatures rise (Figure 9c).

Strengthened cold air advection is associated with increases in ln τ. An increase in cold air advection over a warmer sea surface destabilizes the lower atmosphere, resulting in an increase in surface turbulent heat fluxes which is conducive to enhancing ln τ through increased cloud water content. Since cold air advection is strengthening with global warming (Figure 9b), the net effect of changes in temperature advection is to increase ln τ as global surface air temperatures rise (Figure 9c).

Another important variable that enhances the ln τ of all cloud regimes as it increases is sea surface temperature (SST). Enhanced SSTs encourage mixing of free-tropospheric air into the boundary layer. In the mid-latitudes, where the free-troposphere is relatively moist, entrainment mixing is conducive to an increase in ln τ by enhancing the water content of low-level clouds. At higher latitudes, colder SSTs weaken the mixing of moist free-tropospheric air (Kawai et al., 2017) and therefore may explain the small coefficients (Figure S11 in Supporting Information S1). Because SSTs are actually decreasing locally in the Southern Ocean as the rest of the globe warms (Figure 9b), the net effect of SST is to decrease ln τ in low-cloud regimes over the Southern Ocean (Figure 9c).

Finally, from Figure 9a it is evident that wind speed is an important factor influencing within-regime shifts in ln τ, being the largest overall contributor to cloud optical depth increases with global mean surface temperature changes over most cloud regimes 5–10. The role of a strengthening of wind speed is to consistently increase ln τ across all cloud regimes. Physically, the strengthening of near-surface winds being conducive to cloud formation can be understood as an increase in the rate of evaporation over the Southern Ocean (Boisvert et al., 2020). Furthermore, stronger near-surface winds can also contribute to the lofting of dimethyl sulfate (Bodas-Salcedo et al., 2019) and marine biological aerosols into the atmosphere where they can act as ice-nucleating particles or cloud condensation nuclei in the Southern Ocean (Burrows et al., 2022; DeMott et al., 2015; Wilson et al., 2015). If the particles act as cloud condensation nuclei, this would act to increase ln τ by increasing the particle number concentrations of clouds (Twohy et al., 2021). Conversely, if the particles act as ice-nucleating particles, this would act to decrease τ by decreasing the droplet number concentrations of clouds as droplets freeze or evaporate and contribute to the growth of ice crystals (Vergara-Temprado et al., 2018). Surface wind speed also consistently increases with warming in regions where low-level MODIS cloud regimes occur and is among the most sensitive cloud-controlling factors to global surface temperature changes (Figure 9b). Taken together, the role of surface wind speed plays a dominant role in increasing the optical thickness of low-level clouds with global surface temperature warming (Figure 9c), potentially due to both increases in droplet number concentration and water content.

Summing the contributions of the cloud-controlling factors to $\frac{d \ln \tau}{dT_s}$ within each of the seven MODIS cloud regimes shows that all cloud regimes contribute to increases in cloud optical depth with warming in Figure 9d, which would correspond to a negative cloud feedback since increases in ln τ correspond to more SW reflection back to space and therefore more surface cooling. Omnipresent cloud regime 11 followed by storm track-dominated cloud regimes 6 and 7 contribute most to the increase in ln τ with warming. It should be noted that the change in ln τ values derived from the cloud-controlling factor analysis have been weighted by CF. This means that one should not expect the results shown in Figure 9d to reproduce the positive within-regime cloud optical depth feedback values presented in Figure 8c. The multiple linear regression analysis for individual cloud regimes reliably predicts $\frac{d \ln \tau}{dT_s}$ as shown by the fact that it well reproduces $\frac{d \ln \tau}{dT_s}$ calculated by regressing the change in ln τ on the change in T_s for individual cloud regimes.

Overall, the role of some cloud-controlling factors in determining the low-level cloud optical depth within cloud regimes is quite consistent across cloud regimes over the Southern Ocean; these include the relative humidity at 700 hPa, cold temperature advection, SST and surface wind speed, however, the roles of EIS and downdraft velocity at 700 hPa are more complicated. The low-level cloud regimes 5–10 that exhibit distinct cloud morphologies show that the optical depth of these clouds is overall most sensitive to changes in surface wind speed over the Southern Ocean.

5. Conclusions

The role of cloud morphological changes in the interannual cloud feedback — both changes within and shifts between distinct groups of cloud morphology defined by *cloud regimes* was inferred in this study based on nearly two decades of MODIS and ISCCP satellite observations for the first time. The quantification of cloud morphological changes in the interannual cloud feedback was enabled through the application of the "double decomposition method" (Zelinka et al., 2023) that combines two distinct techniques to diagnose cloud feedbacks that have been applied in the past — the CRK method and the cloud regime method. We focused on λ_τ over the Southern Ocean, invoking additional information to better understand the across-regime and within-regime contributions to the feedback, due to the importance of this feedback in explaining the larger projected warming in contemporary GCMs. Implementation of our novel methodology allows us to isolate shifts between different cloud morphology to

τ thinning with global warming ($\lambda_\tau > 0$) and τ thickening with global warming ($\lambda_\tau < 0$). The main robust conclusions of this study where MODIS and ISCCP agree are summarized below:

- Decreases in thick storm-track and convective clouds and increases in thinner stratocumulus clouds contribute to an overall positive λ_τ in the upper Southern Ocean (55°S to 60°S) region.
- Decreases in thin, low-level clouds and increases in thicker storm-track clouds contribute to a negative λ_τ value over the lower Southern Ocean (60°S to 65°S) region.
- Strengthening near-surface wind speeds robustly increase cloud optical thickness over the Southern Ocean within cloud regimes and play the largest role overall out of the meteorological factors examined in influencing cloud optical thickness in this region.

The double decomposition method has effectively enabled us to diagnose how shifts between different dynamical cloud regimes contribute to the cloud optical depth feedback that would otherwise remain undiagnosed with the CRK method alone. However, a key limitation of the method is that it only tracks cloud regime shifts in an "Eulerian" sense; it is not possible to determine how one particular cloud regime within a grid cell and point in time transformed into another. Furthermore, we acknowledge that there is a level of arbitrariness associated with defining cloud regimes; however, this arbitrariness is inherently present in all techniques used to classify various cloud properties. The general concept of the double decomposition method could also hypothetically be extended to include different definitions of "cloud morphology" in smaller domains, including in global storm resolving models should satellite simulators at higher resolutions be available.

The results of the double decomposition method have implications for evaluating the realism of GCM simulations of cloud regime shifts in a warmer climate. In particular, these satellite-based decomposition of cloud feedbacks can be used to evaluate the ability of GCMs to simulate the interannual cloud feedback if compared in an equivalent fashion, that is, using the relevant satellite simulator, the same time period, and the same analysis methods. Direct comparisons between GCMs and satellite observations can reveal shortcomings in the representation of certain cloud regimes (Chao et al., 2024). It is therefore important that modeling centers continue to or begin to adopt satellite simulators in their simulations and make their output publicly accessible. The across-regime analysis method can reveal which cloud regimes GCMs struggle to represent and shortcomings related to how they are projected to change in a warming climate. Cloud-controlling factor analysis on the within-regime component can reveal the environmental conditions under which clouds are poorly represented. Extension of the current work to include detailed comparisons between satellite observations and consistent GCM experiments using the double decomposition method will be considered in future studies.

Data Availability Statement

MODIS daily cloud histogram data are available from the EarthData landing page (Pincus et al., 2023). The MODIS daily cloud regime data were downloaded from NASA's Goddard Earth Sciences Data and Information Services Center (GES DISC) (Cho et al., 2021b). The ISCCP HGG data set was downloaded from the NOAA website (Rossow et al., 2016). The ISCCP-H weather state data were downloaded from the ISCCP website (Tselioudis et al., 2021b). CERES daily gridded data are available from the CERES website (NASA, 2017). Cloud radiative kernels ("cloud_kernels2.nc") were used for the cloud feedback calculations (Zelinka, 2021). MERRA-2 data were obtained courtesy of GES DISC (GMAO, 2024).

Acknowledgments
I. T., M. D. Z., B. H. K. and L. O. were supported by NASA TASNPP Grant 80NSSC18K1599. M. D. Z.'s work was additionally supported by the U.S. Department of Energy (DOE) Regional and Global Modeling Analysis program area and was performed under the auspices of the DOE by Lawrence Livermore National Laboratory under Contract DE-AC52-07NA27344.A portion of this work was carried out at the Jet Propulsion Laboratory, California Institute of Technology, under a contract with NASA. L. O. and G. T. would like to acknowledge funding from NASA's MEaSUREs program.

References

Ackerman, S. A., Strabala, K., Menzel, P., Frey, R., Moeller, C., Gumley, L., et al. (2006). Discriminating clear-sky from cloud with modis algorithm theoretical basis document (Mod35), version 5.0 [Computer software manual]. https://atmosphere-imager.gsfc.nasa.gov/sites/default/files/ModAtmo/MOD35_ATBD_Collection6_1.pdf

Anderberg, M. R. (1973). *Cluster analysis for applications*. Elsevier.

Betts, A. K., & Harshvardhan. (1987). Thermodynamic constraint on the cloud liquid water feedback in climate models. *Journal of Geophysical Research*, *92*(D7), 8483–8485. https://doi.org/10.1029/jd092id07p08483

Bodas-Salcedo, A., Mulcahy, J. P., Andrews, T., Williams, K. D., Ringer, M. A., Field, P. R., & Elsaesser, G. S. (2019). Strong dependence of atmospheric feedbacks on mixed-phase microphysics and aerosol-cloud interactions in hadGEM3. *Journal of Advances in Modeling Earth Systems*, *11*(6), 1735–1758. https://doi.org/10.1029/2019ms001688

Bodas-Salcedo, A., Web, M. J., Bony, S., Chepfer, H., Dufresne, J. L., Klein, S. A., et al. (2011). COSP: Satellite simulation software for model assessment. *Bulletin of the American Meteorological Society*, *92*(8), 1023–1043. https://doi.org/10.1175/2011bams2856.1

Boisvert, L., Vihma, T., & Shie, C.-L. (2020). Evaporation from the Southern Ocean estimated on the basis of AIRS satellite data. *Journal of Geophysical Research*, *125*(1), e2019JD030845. https://doi.org/10.1029/2019jd030845

Burrows, S. M., MucCluskey, C. S., Gornwell, G., Steinke, I., Zhang, K., Zhao, B., et al. (2022). Ice-nucleating particles that impact clouds and climate: Observational and modeling research needs. *Reviews of Geophysics*, *60*(2), e2021RG000745. https://doi.org/10.1029/2021rg000745

Chan, M. A., & Comiso, J. C. (2013). Arctic cloud characteristics as derived from MODIS, CALIPSO, and CloudSat. *Journal of Climate*, *26*(10), 3285–3306. https://doi.org/10.1175/jcli-d-12-00204.1

Chao, L.-W., Zelinka, M. D., & Dessler, A. E. (2024). Evaluating cloud feedback components in observations and their representation in climate models. *Journal of Geophysical Research*, *129*(2), e2023JD039427. https://doi.org/10.1029/2023jd039427

Cho, N., Tan, J., & Oreopoulos, L. (2021a). Classifying planetary cloudiness with an updated set of MODIS cloud regimes. *Journal of Applied Meteorology and Climatology*, *60*(7), 981–997. https://doi.org/10.1175/jamc-d-20-0247.1

Cho, N., Tan, J., & Oreopoulos, L. (2021b). Modis cloud regime level-3 daily 1 deg x 1 deg, goddard earth sciences data and information services center (ges disc) [dataset]. https://doi.org/10.5067/MEASURES/MODISCR/EQANGD/DATA301

Christensen, M. W., Carrio, G. G., Stephens, G. L., & Cotton, W. R. (2013). Radiative impacts of free-tropospheric clouds on the properties of marine stratocumulus. *Journal of the Atmospheric Sciences*, *70*(10), 3102–3118. https://doi.org/10.1175/jas-d-12-0287.1

Coopman, Q., & Tan, I. (2023). Characterization of the spatial distribution of the thermodynamic phase within mixed-phase clouds using satellite observations. *Geophysical Research Letters*, *50*(24), e2023GL104977. https://doi.org/10.1029/2023gl104977

DeMott, P. J., Hill, T. C. J., McCluskey, C. S., Prather, K. A., Collins, D. B., Sullivan, R. C., et al. (2015). Sea spray aerosol as a unique source of ice nucleating particles. *Proceedings of the National Academy of Sciences*, *113*(21), 5797–5803. https://doi.org/10.1073/pnas.1514034112

Forster, P., Sotrelvmo, T., Armour, K., Collins, W., Dufresne, J.-L., Frame, D., et al. (2021). Climate change 2021: The physical science basis. Contribution of working group i to the sixth assessment report of the intergovernmental panel on climate change. In V. Masson-Delmotte, et al. (Eds.), *The Intergovernmental Panel on Climate Change AR6* (pp. 923–1054). Cambridge University Press.

Frey, W. R., & Kay, J. E. (2018). The influence of extratropical cloud phase and amount feedbacks on climate sensitivity. *Climate Dynamics*, *50*(7–8), 3097–3116. https://doi.org/10.1007/s00382-017-3796-5

Gelaro, R., McCarty, W., arez, M. J. S., Todling, R., Molod, A., Takacs, L., et al. (2017). The modern-era retrospective analysis for research and applications, version 2 (MERRA-2). *Journal of Climate*, *30*(14), 5419–5454. https://doi.org/10.1175/jcli-d-16-0758.1

GMAO. (2024). MERRA-2 Reanalysis (V5.12.4) instantaneous 3-D analyses, at six-hourly intervals reported on pressure levels (inst6_3d_a-na_Np) [dataset]. https://doi.org/10.5067/a7s6xp56vzws

Grosvenor, D. P., & Wood, R. (2014). The effect of solar zenith angle on modis cloud optical and microphysical retrievals within marine liquid water clouds. *Atmospheric Chemistry and Physics*, *14*(14), 7291–7321. https://doi.org/10.5194/acp-14-7291-2014

Haynes, J. M., Jakob, C., Rossow, W. B., Tselioudis, G., & Brown, J. (2011). Major characteristics of southern ocean cloud regimes and their effects on the energy budge. *Journal of Climate*, *24*(19), 5061–5080. https://doi.org/10.1175/2011jcli4052.1

Howard, L. (2011). *Essay on the modifications of clouds*. Cambridge University Press.

Huang, Y., Siems, S. T., Manton, M. J., Protat, A., & Delanoë, J. (2012). A study on the low-altitude clouds over the southern ocean using the DARDAR-MASK. *Journal of Geophysical Research*, *117*(D18204). https://doi.org/10.1029/2012jd017800

Jakob, C., & Tselioudis, G. (2003). Objective identification of cloud regimes in the tropical western pacific. *Geophysical Research Letters*, *30*(21). https://doi.org/10.1029/2003gl018367

Kawai, H., Koshiro, T., & Webb, M. J. (2017). Interpretation of factors controlling low cloud cover and low cloud feedback using a unified predictive index. *Journal of Climate*, *30*(22), 9119–9131. https://doi.org/10.1175/jcli-d-16-0825.1

Kawai, H., Yukimoto, S., Koshiro, T., Oshima, N., Tanaka, T., Yoshimura, H., & Nagasawa, R. (2019). Significant improvement of cloud representation in the global climate model mri-esm2. *Geoscientific Model Development*, *12*(7), 2875–2897. https://doi.org/10.5194/gmd-12-2875-2019

Kelleher, M. K., & Grise, K. M. (2019). Examining southern ocean cloud controlling factors on daily time scales and their connec-tions to midlatitude weather systems. *Journal of Climate*, *34*(14), 5145–5160. https://doi.org/10.1175/jcli-d-18-0840.1

Klein, S. A., Hall, A., Norris, J., & PIncus, R. (2017). Low-cloud feedbacks from cloud-controlling factors: A review. *Surveys in Geophysics*, *38*(6), 1307–1329. https://doi.org/10.1007/s10712-017-9433-3

Lebsock, M., Morrison, H., & Gettelman, A. (2013). Microphysical implications of cloud-precipitation covariance derived from satellite remote sensing. *Journal of Geophysical Research*, *118*(12), 6521–6533. https://doi.org/10.1002/jgrd.50347

Liu, Y., Ackerman, S. A., Maddux, B. C., Key, J. R., & Frey, R. A. (2010). Errors in cloud detection over the arctic using a satellite imager and implications for observing feedback mechanisms. *Journal of Climate*, *23*(7), 1894–1907. https://doi.org/10.1175/2009jcli3386.1

Loeb, N. G., Doelling, D. R., Wang, H., Su, W., Nguyen, C., Corbett, J. G., et al. (2018). Clouds and the earth's radiant energy system (CERES) energy balanced and filled (EBAF) top-of-atmosphere (TOA) edition-4.0 data product. *Journal of Climate*, *31*(1), 895–918. https://doi.org/10.1175/jcli-d-17-0208.1

Mace, G. G., Protat, A., & Benson, S. (2021). Mixed-phase clouds over the southern ocean as observed from satellite and surface based lidar and radar. *Journal of Geophysical Research*, *126*(16), e2021JD034569. https://doi.org/10.1029/2021jd034569

McCoy, D. T., Field, P., Bodas-Salcedo, A., Elsaesser, G. S., & Zelinka, M. D. (2020). A regime-oriented approach to observationally con-straining extratropical shortwave cloud feedbacks. *Journal of Climate*, *33*(23), 9967–9983. https://doi.org/10.1175/jcli-d-19-0987.1

McCoy, D. T., Field, P., Frazer, M. E., Zelinka, M. D., Elsaesser, G. S., Mulmenstadt, J., et al. (2022). Extratropical shortwave cloud feedbacks in the context of the global circulation and hydrological cycle. *Geophysical Research Letters*, *49*(8), e2021GL097154. https://doi.org/10.1029/2021gl097154

McCoy, D. T., Frazer, M. E., Mulmenstadt, J., Tan, I., Terai, C. R., & Zelinka, M. D. (2023). Chapter 6: Extratropical cloud feedbacks in clouds and their climatic impacts. In R. C. Sullivan & C. Hoose (Eds.), *Radiation, circulation, and precipitation*. Wiley.

McCoy, I. L., McCoy, D. T., Wood, R., Zuidema, P., & Bender, F. A. M. (2023). The role of mesoscale cloud morphology in the shortwave cloud feedback. *Geophysical Research Letters*, *50*(2), e2022GL101042. https://doi.org/10.1029/2022gl101042

Mitchell, J. F. B., Senior, C. A., & Ingram, W. J. (1989). CO_2 and climate: A missing feedback? *Nature*, *341*(6238), 132–134. https://doi.org/10.1038/341132a0

Nakajima, T., & King, M. D. (1990). Determination of the optical thickness and effective particle radius of clouds from reflected solar radiation measurements. Part i: Theory. *Journal of the Atmospheric Sciences*, *47*(15), 1878–1893. https://doi.org/10.1175/1520-0469(1990)047<1878:dotota>2.0.co;2

NASA. (2017). CERES and GEO-enhanced TOA, within-atmosphere and surface fluxes, clouds and aerosols monthly terra-aqua Edition4A [Dataset]. *NASA Langley Atmospheric Science Data Center DAAC*. https://doi.org/10.5067/terra+aqua/ceres/syn1degmonth_l3.004a

Naud, C., Elsaesser, G. S., & Booth, J. F. (2023). Dominant cloud controlling factors for low-level cloud fraction: Subtropical versus extratropical oceans. *Geophysical Research Letters*, *50*(19), e2023GL104496. https://doi.org/10.1029/2023gl104496

Norris, J. R., Allen, R. J., Evan, A. T., Zelinka, M. D., O'Dell, C. W., & Klein, S. A. (2016). Evidence for climate change in the satellite cloud record. *Nature*, *536*(7614), 72–75. https://doi.org/10.1038/nature18273

Oreopoulos, L., Cho, N., Lee, D., Kato, S., & Huffman, G. J. (2014). An examination of the nature of global MODIS cloud regimes. *Journal of Geophysical Research*, *119*(13), 8362–8383. https://doi.org/10.1002/2013jd021409

Pincus, R., Hubanks, P. A., Platnick, S., Meyer, K., Holz, R. E., Botambekov, D., & Wall, C. J. (2023). Updated observations of clouds by MODIS for global model assessment. *Earth System Science Data*, *15*(6), 2483–2497. https://doi.org/10.5194/essd-15-2483-2023

Pincus, R., Platnick, S., Ackerman, S. A., Hemler, R., & Hofmann, R. J. P. (2012). Reconciling simulated and observed views of clouds: MODIS, ISCCP, and the limits of instrument simulators. *Journal of Climate*, *25*(13), 4699–4720. https://doi.org/10.1175/jcli-d-11-00267.1

Platnick, S., Meyer, K. G., King, M. D., Wind, G., Amarasinghe, N., Marchant, B., et al. (2016). The MODIS cloud optical and microphysical products: Collection 6 updates and examples from terra and aqua. *IEEE Transactions on Geoscience and Remote Sensing*, *55*(1), 502–525. https://doi.org/10.1109/tgrs.2016.2610522

Pruppacher, H. R., & Klett, J. D. (2012). *Microphysics of clouds and precipitation*. Springer.

Quaas, J. (2012). Evaluating the "critical relative humidity" as a measure of subgrid-scale variability of humidity in general circulation model cloud cover parameterizations using satellite data. *Journal of Geophysical Research*, *117*(D9). https://doi.org/10.1029/2012jd017495

Rossow, W., Walker, A., Golea, V., Knapp, K. R., Young, A., Inamdar, A., & Hankin, B. (2016). International satellite cloud climatology 859 project climate data record, h-series [dataset]. https://www.ncei.noaa.gov/access/metadata/landing-page/bin/iso?id=gov.noaa.ncdc:c00956internationalsatellitecloudclimatologyprojectclimatedatarecord,h-series

Scott, R. C., Myers, T. A., Norris, J. R., Zelinka, M. D., Klein, S. A., Sun, M., & Doelling, D. R. (2020). Observed sensitivity of low-cloud radiative effects to meteorological perturbations over the global oceans. *Journal of Climate*, *33*(18), 7717–7734. https://doi.org/10.1175/jcli-d-19-1028.1

Shell, K. M., Kiehl, J. T., & Shields, C. A. (2008). Using the radiative kernel technique to calculate climate feedbacks in NCAR's community atmospheric model. *Journal of Climate*, *21*(10), 2269–2282. https://doi.org/10.1175/2007jcli2044.1

Soden, B. J., & Donner, L. J. (1994). Evaluation of a GCM cirrus parameterization using satellite observations. *Journal of Geophysical Research*, *99*(D7), 14401–14413. https://doi.org/10.1029/94jd00963

Soden, B. J., Held, I. M., Colman, R., Shell, K. M., Kiehl, J. T., & Shields, C. A. (2008). Quantifying climate feedbacks using radiative kernels. *Journal of Climate*, *21*(14), 3504–3520. https://doi.org/10.1175/2007jcli2110.1

Stevens, B., Bony, S., Brogniez, H., Hentgen, L., Hohenegger, C., Kiemle, C., et al. (2019). Sugar, gravel, fish and flowers: Mesoscale cloud patterns in the trade winds. *Quarterly Journal of the Royal Meteorological Society*, *146*(726), 141–152. https://doi.org/10.1002/qj.3662

Stevens, B., & Brenguier, J.-L. (2009). In J. Heintzenberg & R. J. Charlson (Eds.), *Clouds in the perturbed climate system: Their relationship to energy balance, atmospheric dynamics, and precipitation: Cloud-controlling factors: Low clouds*. MIT Press Cambridge.

Su, H., Jiang, J. H., Zhai, C., Perun, V. S., Shen, J. T., Genio, A. D., et al. (2013). Diagnosis of regime-dependent cloud simulation errors in CMIP5 models using "a-train" satellite observations and reanalysis data. *Journal of Geophysical Research*, *118*(7), 2762–2780. https://doi.org/10.1029/2012jd018575

Sun, Z., & Shine, K. P. (1994). Studies of the radiative properties of ice and mixed-phase clouds. *Quarterly Journal of the Royal Meteorological Society*, *120*(515), 111–137. https://doi.org/10.1002/qj.49712051508

Tan, I., Oreopoulos, L., & Cho, N. (2019). The role of thermodynamic phase shifts in cloud optical depth variations with temperature. *Geophysical Research Letters*, *46*(8), 4502–4511. https://doi.org/10.1029/2018gl081590

Tan, I., Storelvmo, T., & Zelinka, M. D. (2016). Observational constraints on mixed-phase clouds imply higher climate sensitivity. *Science*, *352*(6282), 224–227. https://doi.org/10.1126/science.aad5300

Terai, C. R., Klein, S. A., & Zelinka, M. D. (2016). Constraining the low-cloud optical depth feedback at middle and high latitudes using satellite observations. *Journal of Geophysical Research*, *121*(16), 9696–9716. https://doi.org/10.1002/2016jd025233

Tselioudis, G., Rossow, W. B., Jakob, C., Remillard, J., Tropf, D., & Zhang, Y. (2021a). Evaluation of clouds, radiation, and precipitation in CMIP6 models using global weather states derived from ISCCP-H cloud property data. *Journal of Climate*, *34*(17), 7311–7324. https://doi.org/10.1175/jcli-d-21-0076.1

Tselioudis, G., Rossow, W. B., Jakob, C., Remillard, J., Tropf, D., & Zhang, Y. (2021b). Global weather states from ISCCP HGG cloud dataset [dataset]. http://isccp.giss.nasa.gov/wstates/hggws.html

Tselioudis, G., Rossow, W. B., & Rind, D. (1992). Global patterns of cloud optical thickness variation with temperature. *Journal of Climate*, *5*(12), 1484–1495. https://doi.org/10.1175/1520-0442(1992)005<1484:gpocot>2.0.co;2

Tsushima, Y., Emori, S., Ogura, T., Kimoto, M., Webb, M. J., Williams, K. D., et al. (2006). Importance of the mixed-phase cloud distribution in the control climate for assessing the response of clouds to carbon dioxide increase: A multi-model study. *Climate Dynamics*, *27*(2–3), 113–126. https://doi.org/10.1007/s00382-006-0127-7

Tsushima, Y., Ringer, M. A., Koshiro, T., Kawai, H., Roehrig, R., Cole, J., et al. (2015). Robustness, uncertainties, and emergent constraints in the radiative responses of stratocumulus cloud regimes to future warming. *Climate Dynamics*, *46*(9–10), 3025–3039. https://doi.org/10.1007/s00382-015-2750-7

Twohy, C. H., DeMott, P. J., Russell, L. M., Toohey, D. W., Rainwater, B., Geiss, R., et al. (2021). Cloud-nucleating particles over the southern ocean in a changing climate. *Earth's Future*, *9*(3), e2020EF001673. https://doi.org/10.1029/2020ef001673

Vergara-Temprado, J., Miltenberger, A. K., Furtado, K., Grosvenor, D. P., Shipway, B. J., Hill, A. A., et al. (2018). Strong control of Southern Ocean cloud reflectivity by ice-nucleating particles. *Proceedings of the National Academy of Sciences*, *115*(11), 2687–2692. https://doi.org/10.1073/pnas.1721627115

Wall, C. J., Storelvmo, T., Norris, J. R., & Tan, I. (2022). Observational constraints on southern ocean cloud-phase feedback. *Journal of Climate*, *35*(15), 5087–5102. https://doi.org/10.1175/jcli-d-21-0812.1

Wang, X., Miao, H., Liu, Y., Bao, Q., He, B., Li, J., & Zhao, Y. (2022). The use of satellite data-based "critical relative humidity" in cloud parameterization and its role in modulating cloud feedback. *Journal of Advances in Modeling Earth Systems*, *14*(10), e2022MS003213. https://doi.org/10.1029/2022ms003213

Wetherald, R. T., & Manabe, S. (1988). Cloud feedback processes in a general circulation model. *Journal of the Atmospheric Sciences*, *45*(8), 1397–1415. https://doi.org/10.1175/1520-0469(1988)045<1397:cfpiag>2.0.co;2

Williams, K. D., & Tselioudis, G. (2007). GCM intercomparison of global cloud regimes: Present-day evaluation and climate change response. *Climate Dynamics*, *29*(2–3), 231–250. https://doi.org/10.1007/s00382-007-0232-2

Williams, K. D., & Webb, M. J. (2009). A quantitative performance assessment of cloud regimes in climate models. *Climate Dynamics*, *33*(1), 141–157. https://doi.org/10.1007/s00382-008-0443-1

Wilson, T. D., Ladino, L. A., Alpert, P. A., Breckels, M. N., Brooks, I. M., Brose, J., et al. (2015). A marine biogenic source of atmospheric ice-nucleating particles. *Nature*, *525*(7568), 234–238. https://doi.org/10.1038/nature14986

Wood, R., & Bretherton, C. S. (2006). On the relationship between stratiform low cloud cover and lower-tropospheric stability. *Journal of Climate*, *19*(24), 6425–6432. https://doi.org/10.1175/jcli3988.1

Wood, R., & Hartmann, D. L. (2006). Spatial variability of liquid water path in marine low cloud: The importance of mesoscale cellular convection. *Journal of Climate*, *19*(9), 1748–1764. https://doi.org/10.1175/jcli3702.1

Young, A. H., Knapp, K. R., Inamdar, A., Hankins, W., & Rossow, W. B. (2018). The international satellite cloud climatology project h-series climate data record product. *Earth System Science Data*, *10*(1), 583–593. https://doi.org/10.5194/essd-10-583-2018

Zelinka, M. D. (2021). mzelinka/cloud-radiative-kernels: Release (v1.0) [dataset]. *Zenodo*. https://doi.org/10.5281/zenodo.5514137

Zelinka, M. D., Klein, S. A., & Hartmann, D. L. (2012). Computing and partitioning cloud feedbacks using cloud property histograms. Part I: Cloud radiative kernels. *Journal of Climate*, *25*(11), 3715–3735. https://doi.org/10.1175/jcli-d-11-00248.1

Zelinka, M. D., Klein, S. A., Taylor, K. E., Andrews, T., Webb, M. J., Gregory, J. M., & Forster, P. M. (2013). Contributions of different cloud types to feedbacks and rapid adjustments in CMIP5. *Journal of Climate*, *26*(14), 5007–5027. https://doi.org/10.1175/jcli-d-12-00555.1

Zelinka, M. D., Myers, T. A., McCoy, D. T., Po-Chedley, S., Caldwell, P. M., Ceppi, P., et al. (2020). Causes of higher climate sensitivity in CMIP6 models. *Geophysical Research Letters*, *47*(1), e2019GL085782. https://doi.org/10.1029/2019gl085782

Zelinka, M. D., Tan, I., Oreopoulos, L., & Tselioudis, G. (2023). Detailing cloud property feedbacks with a regime-based decomposition. *Climate Dynamics*, *60*(9–10), 2983–3003. https://doi.org/10.1007/s00382-022-06488-7

Zhang, M. H., Lin, W. Y., Klein, S. A., Bacmeister, J. T., Bony, S., Cederwall, R. T., et al. (2005). Comparing clouds and their seasonal variations in 10 atmospheric general circulation models with satellite measurements. *Journal of Geophysical Research*, *110*(D15S02). https://doi.org/10.1029/2004jd005021

Zhang, Z., Oreopoulos, L., Lebsock, M. D., Mechem, D. B., & Covert, J. (2022). Understanding the microphysical control and spatial-temporal variability of warm rain probability using cloudsat and MODIS observations. *Geophysical Research Letters*, *49*(10), e2022GL098863. https://doi.org/10.1029/2022gl098863

Zhou, C., Zelinka, M. D., Dessler, A. E., & Klein, S. A. (2016). The relationship between interannual and long-term cloud feedbacks. *Geophysical Research Letters*, *42*(23), 10463–10469. https://doi.org/10.1002/2015gl066698